

Multiplicity dependence of (multi)strange hadrons in oxygen-oxygen collisions at $\sqrt{s_{NN}} = 7$ TeV using EPOS4 and AMPT

M. U. Ashraf,^{1,*} A. M. Khan,^{2,†} J. Singh,^{3,‡} N. Kumar,⁴ G. Nigmatkulov,⁵ and S. Kabana³

¹*Department of Physics and Astronomy, Wayne State University,
666 W. Hancock, Detroit, Michigan 48201, USA*

²*Georgia State University, Atlanta, GA 30303, USA*

³*Instituto de Alta Investigación, Universidad de Tarapacá, Casilla 7D, Arica, 1000000, Chile*

⁴*Department of Physics, Panjab University, Chandigarh 160014, India*

⁵*Department of Physics, University of Illinois Chicago, Chicago, IL 60607, USA*

(Dated: January 22, 2025)

It is anticipated that the Large Hadron Collider (LHC) will collect data from oxygen-oxygen (O + O) collisions at a center-of-mass energy of $\sqrt{s_{NN}} = 7$ TeV to explore the effects observed in high multiplicity proton-proton (p + p) and proton-lead (p + Pb) collisions that closely related to lead-lead (Pb + Pb) collisions. These effects include azimuthal asymmetries in particle production, as well as variations in the abundances and momentum distributions across different hadron species, which are indicative of collective particle production mechanisms induced by the interactions in the presence of a QGP. The upcoming data on O+O collisions at the LHC are expected to constrain the model parameters and refine our understanding of theoretical models. In this work, the predicted transverse momentum (p_T) spectra, rapidity density distributions (dN/dy), particle yield ratios, and p_T -differential ratios of (multi)strange hadrons produced in O + O collisions at $\sqrt{s_{NN}} = 7$ TeV using AMPT and EPOS4 models are presented. AMPT focuses on preformed hadronic interactions, while EPOS4 incorporates a QGP phase. Stronger radial flow in EPOS4 as compared to AMPT is also observed. AMPT incorporates some flow effects, but the implementation of full hydrodynamic flow in EPOS4 appears to be significantly more effective in reproducing the existing experimental data. Both models predict the final state multiplicity overlap with p + p, p + Pb, and Pb + Pb collisions.

I. INTRODUCTION

High-energy heavy-ion collisions provide an opportunity to create and study the Quark-Gluon Plasma (QGP) — a strongly interacting state of matter that is described by a Quantum Chromodynamics (QCD) [1–3]. In recent years, there has been a lot of debate about the limit of the smallest possible droplet of the QGP that could be formed in collisions. Experiments at the Relativistic Heavy Ion Collider (RHIC) and the Large Hadron Collider (LHC) have facilitated the investigations on the properties of the QGP. Collisions of symmetric heavy-ions, such as lead-lead (Pb+Pb) and gold-gold (Au+Au), at these facilities have revealed that the QGP exhibits hydrodynamic behavior, flowing like a nearly perfect fluid with large entropy-density-to-viscosity ratio [4, 5]. This interpretation of nucleus-nucleus (A + A) results depends on the comparison with the results from small collision systems, such as proton-proton (p + p) or proton-nucleus (p + A) because it allows to identify and understand the nuclear effects and final state phenomena in large systems.

Strangeness enhancement has been widely recognized and observed as a key signature of the Quark-Gluon Plasma (QGP), as the hot medium facilitates the thermal

production of strange quarks [6].

The ratios of production yields for various strange hadrons relative to pions in A + A collisions from SPS to LHC show significant centrality and energy dependence [7]. Recent studies [8, 9] at the LHC have observed features such as azimuthal anisotropies, modified hadron yields, and spectra in high-multiplicity p + p and p + Pb collisions that are surprisingly similar to those observed in A + A collisions, despite the significant difference in system size [8, 10]. These findings also exhibit qualitative agreement with the predictions of the statistical hadronization model (SHM) [11]. The model describes particle production in terms of thermal equilibrium without the QGP formation [12–15].

These findings are also consistent with the core-corona model [16–20] based on the assumption that strange quarks are produced thermally in the core, a high-density region of the colliding nuclei. On the other hand, the most commonly used Monte Carlo (MC) models for p + p collisions like Pythia [21, 22] and EPOS-LHC [23] are unable to quantitatively describe the strangeness enhancement observed in the existing experimental data [8]. These observations present a significant challenge to a current theoretical understanding of QGP formation, as they suggest the possibility of QGP-like behavior in smaller collision systems than previously anticipated. Consequently, to understand the enhanced production of strange hadrons in small systems, both experimental investigation and advancement in hydrodynamic and transport models are required. The hydrodynamic and

* muashraf@wayne.edu;

† ahsan.mehmood.khan@cern.ch;

‡ jsingh2@bnl.gov;

TABLE I. Average charged-particle multiplicity ($\langle dN_{\text{ch}}/d\eta \rangle$) at $|\eta| < 0.5$ and $\langle N_{\text{part}} \rangle$ in O + O collisions at $\sqrt{s_{\text{NN}}} = 7$ TeV for different centrality classes using AMPT-Def, AMPT-SM and EPOS4.

Centrality (%)	AMPT-Def		AMPT-SM		EPOS	
	$\langle dN_{\text{ch}}/d\eta \rangle \pm \text{rms}$	$\langle N_{\text{part}} \rangle \pm \text{rms}$	$\langle dN_{\text{ch}}/d\eta \rangle \pm \text{rms}$	$\langle N_{\text{part}} \rangle \pm \text{rms}$	$\langle dN_{\text{ch}}/d\eta \rangle \pm \text{rms}$	$\langle N_{\text{part}} \rangle \pm \text{rms}$
0 – 5	185.556 ± 0.016	28.82 ± 2.12	188.293 ± 0.043	29.00 ± 2.03	236.440 ± 0.142	27.86 ± 2.18
5 – 10	142.550 ± 0.015	26.35 ± 2.69	145.678 ± 0.038	26.78 ± 2.60	189.801 ± 0.130	25.05 ± 2.33
10 – 20	108.771 ± 0.009	22.77 ± 3.28	110.442 ± 0.023	23.24 ± 3.24	148.437 ± 0.083	21.44 ± 3.15
20 – 30	75.674 ± 0.008	18.13 ± 3.29	76.085 ± 0.019	18.54 ± 3.26	105.863 ± 0.071	16.87 ± 3.12
30 – 40	51.864 ± 0.006	14.03 ± 3.08	51.471 ± 0.016	14.33 ± 3.05	75.027 ± 0.064	12.44 ± 2.56
40 – 50	34.789 ± 0.005	10.58 ± 2.79	34.188 ± 0.013	10.80 ± 2.75	53.037 ± 0.050	9.60 ± 2.52
50 – 60	22.701 ± 0.004	7.84 ± 2.42	22.082 ± 0.010	7.99 ± 2.40	37.146 ± 0.062	6.98 ± 2.30
60 – 80	11.493 ± 0.002	4.86 ± 1.99	11.117 ± 0.005	4.94 ± 2.00	19.889 ± 0.023	4.49 ± 1.96
80 – 100	3.860 ± 0.001	2.60 ± 1.01	3.761 ± 0.003	2.63 ± 1.03	5.127 ± 0.011	1.89 ± 1.53

transport approaches complement each other. Hydrodynamic models provide direct access to the equation of state and transport coefficients, while transport models can address non-equilibrium dynamics and provide a microscopic picture of the interactions [24].

To further the understand QGP formation mechanisms in small systems, LHC experiments are anticipated to collect data from oxygen-oxygen (O + O) collisions at $\sqrt{s_{\text{NN}}} = 7$ TeV [25, 26]. This offers a significant and timely opportunity to investigate these effects in a system with a small number of participating nucleons and a final-state multiplicity comparable to that of smaller systems but with a larger geometrical transverse overlap. Strangeness production studies in O + O collisions, in a multiplicity range that bridges p + p and p + Pb on the low side, and Pb + Pb and Xe + Xe on the high side [26], are of primary interest for determining the hadrochemistry of the formed medium and for studying hadronization. The underlying mechanisms of particle production in O + O collisions have recently been explored in several theoretical studies [27–36].

The predictions presented in this work are based on the recently updated versions of the EPOS (EPOS4) and AMPT models. The EPOS4 reasonably reproduces the overall strangeness enhancement observed in the ALICE data [37]. At the same time, AMPT does not provide a consistent description of the yields and p_{T} spectra of multistrange baryons in heavy-ion collisions [38]. Both models employ different mechanisms for strangeness production. EPOS4 includes the QGP phase in its hydrodynamic evolution with the lattice QCD equation of state (EoS). AMPT, on the other hand, does not have a fully chemically equilibrated system as compared to EPOS4. The partonic stage in AMPT is described by a parton cascade where interactions are primarily 2-to-2 elastic scatterings. In AMPT, the system can be isotropic in momentum space but not chemically equilibrated. In this article, we report on the predictions of various strange hadron (K_{S}^0 , Λ ($\bar{\Lambda}$), $\Xi^- + \bar{\Xi}^+$, $\Omega^- + \bar{\Omega}^+$, and ϕ) production in O + O collisions at $\sqrt{s_{\text{NN}}} = 7$ TeV using the AMPT [39, 40] and EPOS4 [37, 41, 42] models.

The observables under study include p_{T} spectra, rapidity density distributions (dN/dy), multiplicity dependence of the yield ratios of strange hadrons relative to pions, and p_{T} -differential strange-baryon-to-meson ratios.

The paper is organized as follows. In Section I, the importance of O + O collisions is described. Section II briefly presents event generation methodology with the AMPT and EPOS4 models. The results are reported and discussed in Section III. The summary, primary findings, and potential outlook for future research are given in Section IV.

II. EVENT GENERATORS

The section provides a short description of the AMPT and EPOS4 models. The multiplicity classes in these predictions are based on the pseudorapidity distribution of charged particles within the region $|\eta| < 0.5$, following the same approach used in the experimental data [13]. The corresponding $\langle dN_{\text{ch}}/d\eta \rangle$ and $\langle N_{\text{part}} \rangle$ values for different centrality classes for both models are given in Table I.

A. AMPT

The AMPT model was developed to study the dynamics of relativistic heavy-ion collisions and has been extensively used for various studies at RHIC and LHC energies [39, 40]. Both default (AMPT-Def) and string melting (AMPT-SM) versions have been utilized in this work. In AMPT, the HIJING model [43] provides the initial spatial and momentum distributions of minijet partons and soft string excitations. The subsequent space-time evolution of these partons is then governed by the ZPC parton cascade model [44]. Following the parton cascade evolution, the model transitions the remaining partonic degrees of freedom into final-state hadrons using either string fragmentation or quark coalescence mechanisms. Subsequently, the interactions of these newly

formed hadrons are governed by the Hadronic Transport Model (ART) [45].

The default version of the AMPT model reasonably reproduces the rapidity distributions and p_T spectra of identified particles at SPS and RHIC energies. This is due to the fact that it only involves minijet partons from HIJING in the parton cascade and uses the Lund string fragmentation for the hadronization [21]. However, the default version significantly underestimates elliptic flow at RHIC energies [46]. In AMPT-SM, the initial hadrons produced by the Lund string fragmentation are converted to their valence quarks [46]. A simple quark coalescence model is then employed to convert these quarks back into hadrons after the ZPC. This approach has been successful in describing anisotropic flow in both large and small collision systems [46–48].

In this study, we analyzed ~ 6 million minimum-bias events for both AMPT-Def and AMPT-SM.

B. EPOS4

EPOS4 is a multipurpose event generator that uses a unique approach to treat all systems ($p + p$, $p + A$ and $A + A$). The EPOS model simulates nucleus-nucleus ($A + A$) collisions using a 3+1 dimensional viscous hydrodynamic approach [16]. The initial conditions in EPOS4 are defined in terms of flux tubes using the Gribov-Regge multiple scattering theory [49]. The core-corona, hydrodynamical evolution, and the hadronic cascade are the three main components of EPOS4. The fragmentation of flux tubes into core and corona (which later hadronize into hadron jets) is determined by the probability of a fragment escaping the bulk matter. This probability depends on the transverse momentum of a fragment and the local string density. EPOS4 [37] further incorporates a mechanism to distinguish between the core and corona zones of particle production within the colliding nuclei. To account for the density variations within the system, Regge theory [49] is used for the low density (corona), and hydrodynamic equations are used for the high density (core). The core utilizes a Cooper-Frye procedure to transition from the fluid to the particles. The vHLLE algorithm [50], a viscous hydrodynamic approach implemented in a 3+1D framework, is employed with an equation of state derived from lattice QCD. The hadronic afterburner, a hadronic cascade model based on the UrQMD model [51, 52], is employed to describe the late stages [51–53].

The core-corona model reproduces many features of $p + p$ and $Pb + Pb$ collisions [37]. Including the core-corona distinction improved the description of the centrality dependence of resonance production and strange particle production in $A + A$ collisions [54]. Additional details regarding the EPOS4 version used in this work can be found in Ref. [37].

A total of ~ 3 million minimum-bias events were simulated from EPOS4. The simulations were conducted

with specific parameters. To incorporate core-corona effects, the “full” core option was activated. Furthermore, the “hydro” parameter was enabled to model hydrodynamic evolution, describing the collective particle flow. The equation of state (EoS) was the standard 3-flavor crossover EoS that is consistent with the lattice QCD calculations at zero net density [55]. The hadronic cascade, the interactions between particles after the initial collision, was enabled.

III. RESULTS AND DISCUSSION

The transverse momentum (p_T) distributions of K_S^0 , Λ , Ξ , ϕ , and Ω from AMPT-Def, AMPT-SM, and EPOS4 in the most central (0–5%) and most peripheral (60–80%) O + O collisions at $\sqrt{s_{NN}} = 7$ TeV are shown in Fig. 1. The EPOS4 results are depicted by solid lines in Fig. 1 (left). In contrast, the AMPT-Def and AMPT-SM model results are represented by dotted and solid lines, respectively, in Fig. 1 (right).

The p_T distributions of different particle species exhibit a clear evolution with centrality as well as particle type. At low p_T , the distributions tend to flatten, with this effect being stronger for heavier particles than lighter ones, demonstrating a mass ordering behavior. This is expected in hydrodynamic models as a consequence of the blue shift induced by the collective expansion of the system. At intermediate p_T , the spectra of heavier particles seem to converge with those of lighter particles. This may be attributed to radial flow. As the system expands, the radial flow can impart additional momentum to particles with lower p_T , pushing them towards intermediate- p_T region [56, 57]. The slope of the p_T -spectra generally becomes harder with the increase in centrality, and it is evident in Fig. 1. In 0–5% central collisions, the decrease in the slope of p_T spectra is more pronounced in comparison with the 60–80% peripheral collisions, indicating the presence of stronger radial flow. Furthermore, heavier particles exhibit a significantly flatter slope as compared to lighter particles, which is consistent with an increase in radial flow with increasing particle mass. A similar trend has been observed in the p_T spectra of identified hadrons in O + O collisions using EPOS4 [36].

The production of strange hadrons at low p_T in AMPT and EPOS4 is driven by different mechanisms. The shape of the spectra is more influenced by partonic scatterings and hadronic rescatterings in AMPT, while hydrodynamic evolution plays a dominant role in EPOS4. As a result, EPOS4 exhibits stronger radial flow than AMPT. At intermediate p_T , the AMPT-SM model, which includes quark coalescence, typically exhibits a peak in the p_T spectra, reflecting the transition from thermal to coalescence-dominated production. Conversely, EPOS4, incorporating collective flow, viscous hydrodynamics, and fragmentation-recombination hadronization. It generally produces smoother p_T spectra. In the high- p_T region, particles in AMPT are pri-

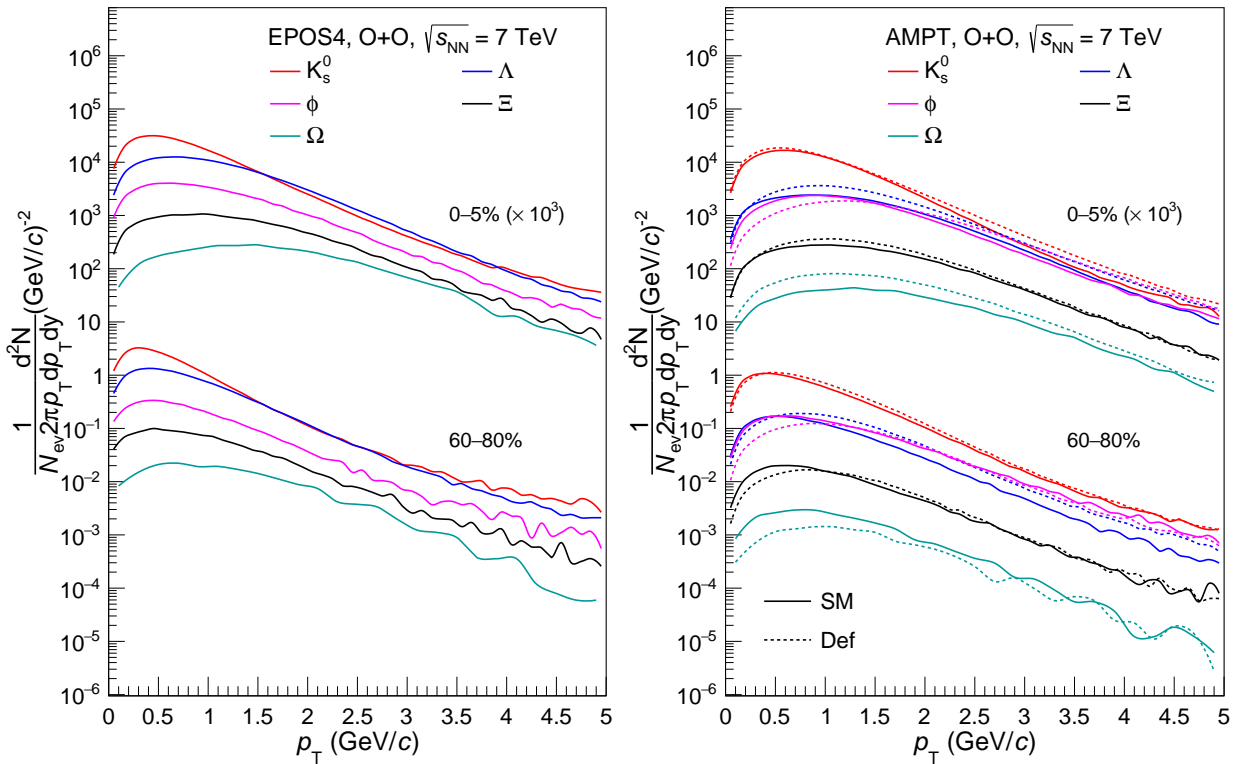


FIG. 1. (Color online) p_T -spectra of (multi)strange hadrons (K_s^0 , Λ , Ξ , ϕ and Ω) from EPOS4 (left) and AMPT (right) in O + O collisions at $\sqrt{s_{NN}} = 7$ TeV for most central (0–5%) and most peripheral (60–80%) centrality classes. 0–5% p_T spectra for (multi)strange hadrons are scaled by a factor of 10 for better visualization. In the right-side figure, solid lines represent AMPT-SM, while dotted lines represent AMPT-Def.

marily produced through minijets or jets, followed by hadronization. The treatment of jet energy loss in AMPT can influence the suppression of high- p_T hadrons. In contrast, EPOS4 considers core-corona separation, which affects the high- p_T region of the spectra. The corona region (non-hydrodynamic) generates high- p_T particles via jet fragmentation, while the core region produces lower p_T particles through hydrodynamics. Consequently, EPOS4 may exhibit slightly different suppression patterns for high- p_T hadrons as compared to AMPT.

Figure 2 shows the predictions from the same models for the yields (dN/dy) of various strange hadrons as a function of event charged-particle multiplicity density ($\langle dN_{ch}/d\eta \rangle$). The predictions from both models show an increasing trend in the yield of strange hadrons as we move from central to peripheral collisions, indicating the strong multiplicity dependence. It is also observed that the average yields of multi-strange hyperons decrease systematically with increasing number of strange quarks. In EPOS4, the central collisions are always core-dominated, and the contribution of the core becomes less and less with decreasing centrality [58]. It is observed that heavier particles show strong centrality dependence as compared to lighter particles. In EPOS4, the strength of centrality dependence varies based on the hadron type, for instance, Ξ and Ω exhibit a stronger centrality de-

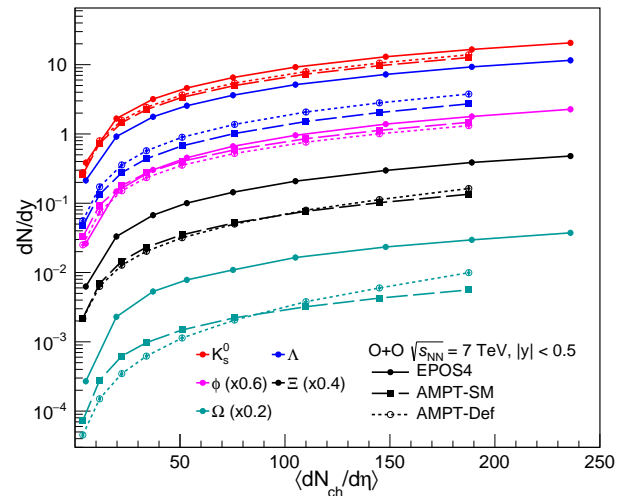


FIG. 2. (Color online) Multiplicity dependence of particle yield (dN/dy) of strange hadrons (K_s^0 , Λ , Ξ , ϕ , and Ω) in O + O collisions at $\sqrt{s_{NN}} = 7$ TeV using AMPT-Def, AMPT-SM and EPOS4. Solid lines are used for EPOS4, whereas the dotted and dashed lines represent AMPT-Def and AMPT-SM, respectively.

pendence compared to K_S^0 . The centrality dependence appears to be primarily determined by the relative significance of the corona contribution. As the contribution of corona diminishes, the yield variation with centrality becomes more pronounced [58]. All models consistently predict an increase in dN/dy with increasing $\langle dN_{ch}/d\eta \rangle$. The predictions for Λ , Ξ , and Ω by EPOS4 are always larger than those from the AMPT-Def and AMPT-SM.

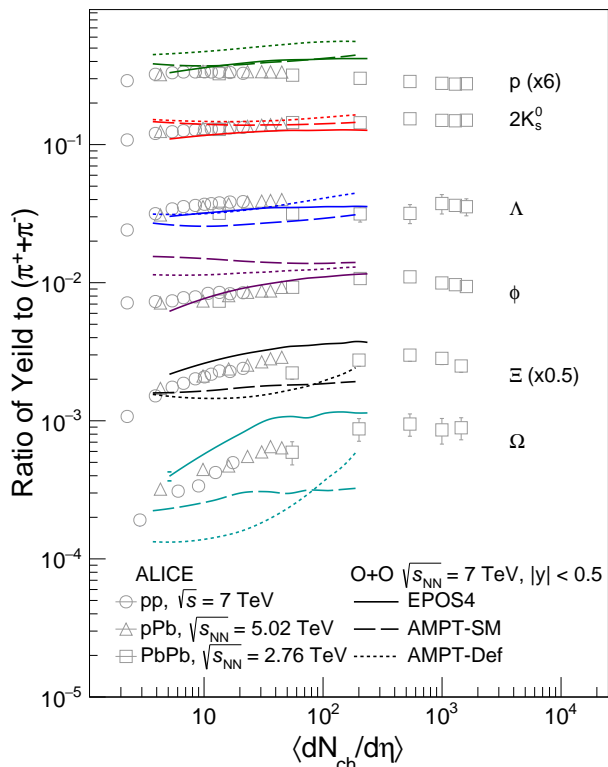


FIG. 3. (Color online) p_T -integrated yield ratios of K_S^0 , Λ , Ξ , ϕ , and Ω to pions ($\pi^+ + \pi^-$) as a function of $\langle dN_{ch}/d\eta \rangle$ in O+O collisions at $\sqrt{s_{NN}} = 7$ TeV using AMPT-Def, AMPT-SM and EPOS4. Solid lines are used for EPOS4, whereas the dotted and dashed lines represent the AMPT-Def and AMPT-SM models, respectively. The values are compared to the published results from p + p, p + Pb, and Pb + Pb collisions [8, 59–63].

To investigate the relative production of strange particles with respect to non-strange particles, the yield ratios of strange particles to pions were calculated as a function of charged particle multiplicity, and the predictions from all the models are shown in Fig. 3. In AMPT-Def, the mechanism of string fragmentation is responsible for hadronization. This process involves the fragmentation of color strings connecting quarks and antiquarks, resulting in the production of strange hadrons. As string fragmentation does not fully account for the collective flow, it underestimates strangeness production as compared to models that include quark coalescence, like AMPT-SM [64]. The p_T -integrated ratios of strange hadrons over pions in the AMPT-Def are less sensitive to the multiplicity

because the production of strange quarks is sensitive to fragmentation rather than collective effects. In the AMPT-SM, quarks are produced as partons after parton-parton scatterings, and hadronization occurs via quark coalescence. This version better simulates the creation of a dense medium similar to the QGP, making it more likely to exhibit strangeness enhancement. As charged-particle multiplicity increases, quarks in the AMPT-SM model are more likely to recombine into strange hadrons, leading to a significant increase in the yield ratios of K_S^0 , Λ , Ξ , ϕ and Ω over pions. The enhancement of strange hadrons is more pronounced due to the more favorable environment for strange quark coalescence at higher multiplicities. AMPT simulations suggest that 0–5% centrality in O + O collisions corresponds to a charged-particle multiplicity similar to that observed in 50–60% centrality in Pb + Pb collisions.

EPOS4 includes a detailed description of the collision dynamics through viscous hydrodynamics, which is crucial for modeling the medium’s collective behavior and its effect on particle production. The medium formed in EPOS4 experiences significant flow effects, and hadronization is modeled through both fragmentation and quark coalescence depending on the core-corona separation. As charged-particle multiplicity increases, the “core” region dominates the collision. In this region, strange quarks are more likely to be produced due to the high energy density and temperature, leading to a clear strangeness enhancement. EPOS4 combines hydrodynamic evolution and statistical hadronization, leading to predictions that the ratios of strange hadrons over pions, particularly for multistrange hadrons (Ξ and Ω), increase significantly with charged-particle multiplicity. This is due to the larger number of strange quarks in the core region that can coalesce into multistrange baryons and mesons. In low-multiplicity events, the corona region of EPOS4, where hard processes such as jet fragmentation dominate, generates a reduced number of strange quarks. Consequently, the ratios of strange hadrons relative to pions are lower than high-multiplicity events, where the core region dominates, and strangeness is enhanced. The predictions of the yield ratios relative to pions in O + O collisions from all models are compared with those measured in p + p, p + Pb, and Pb + Pb collisions at available LHC energies [8, 59–63]. Interestingly, these predictions from all models shows a clear final state multiplicity overlap with p + p, p + Pb, and Pb + Pb collisions.

Figure 4 shows the p_T -differential particle ratios (K/π and Λ/π) in the most central (0–5%) and the most peripheral (60–80%) O+O collisions at $\sqrt{s_{NN}} = 7$ TeV using all models. Particle ratios involving different hadron species serve as a direct probe of the relative abundances and interaction dynamics of the underlying quark constituents within the hot and dense medium. Both ratios serve as a measure of the strangeness enhancement and are observed for both EPOS4 and AMPT models at intermediate p_T . This enhancement shows weak centrality

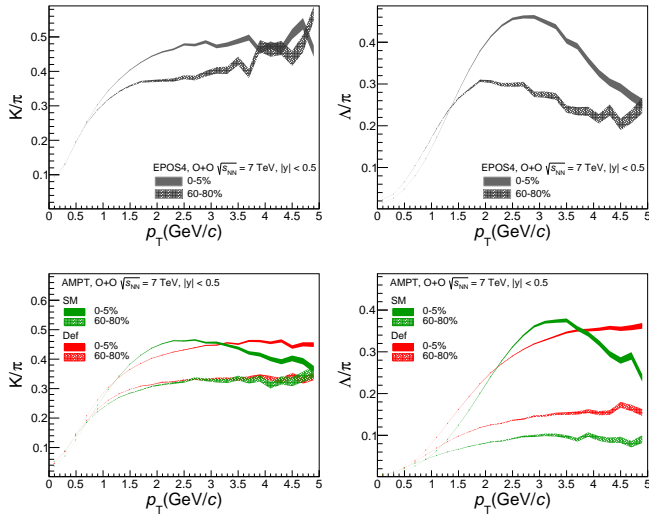


FIG. 4. (Color online) p_T -differential K/π and Λ/π ratios in most central (0–5%) and the most peripheral (60–80%) O + O collisions at $\sqrt{s_{NN}} = 7$ TeV using EPOS4 (top) and AMPT (bottom). Black color is used for EPOS4, whereas the red and green colors represent AMPT-Def and the AMPT-SM model, respectively. The solid and dashed bands represent the ratios at the most central (0–5%) and most peripheral (60–80%) centrality classes, respectively.

dependence at low p_T while exhibiting strong centrality dependence at the intermediate- p_T region. The production of strangeness is maximum for the central collisions at intermediate- p_T , while it decreases with centrality. Λ/π ratio also exhibits similar behavior due to similar strangeness content in K and Λ . Additionally, Λ/π ratios from EPOS4 and AMPT-SM show a clear peak around 2–3 GeV/ c , and this peak is more pronounced in most central collisions. The strangeness enhancement observed in the K/π ratio at intermediate p_T for EPOS4 exhibits qualitative agreement with the AMPT-SM model. However, the Λ/π ratio predicted by EPOS4 is slightly larger than that in AMPT-Def and AMPT-SM due to stronger radial flow in central collisions.

Figure 5 shows the ϕ/π and Ξ/π ratios in the most central (0–5%) and peripheral (60–80%) O + O collisions at $\sqrt{s_{NN}} = 7$ TeV using EPOS4, AMPT-Def, and AMPT-SM models. The rise in ϕ/π and Ξ/π ratios is more gradual, exhibiting a rapid increase at low p_T as compared to K/π and Λ/π ratios. Both ratios show weak centrality dependence at low p_T but strong centrality dependence at intermediate- p_T from all models. It is observed that at intermediate p_T , the ϕ/π ratio is twice as large for AMPT-SM as compared to EPOS4 in the most central collisions. This may be due to the fact that, at the intermediate- p_T region where the momentum of a particle becomes comparable or more than the mass of strange quark, the production probability of $s\bar{s}$ increases significantly. Additionally, ϕ mesons are not only produced from the fragmentation of excited strings in the initial collisions but also from the hadronic mat-

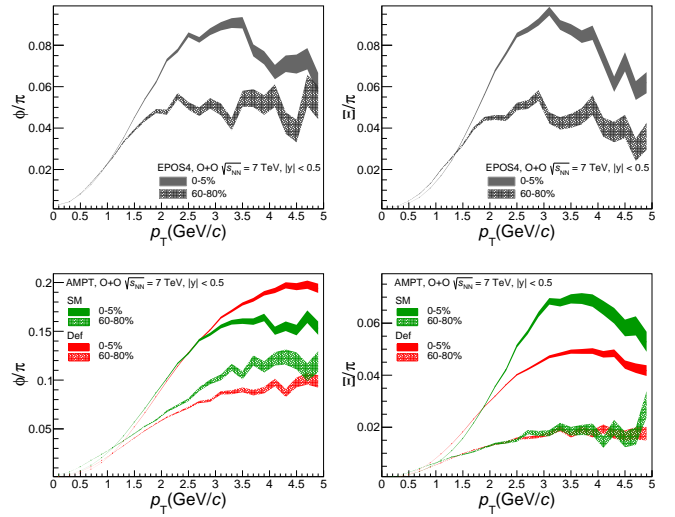


FIG. 5. (Color online) p_T -differential ϕ/π and Ξ/π ratios in most central (0–5%) and the most peripheral (60–80%) O + O collisions at $\sqrt{s_{NN}} = 7$ TeV using EPOS4 (top) and AMPT (bottom). Black color is used for EPOS4, whereas the red and green colors represent AMPT-Def and the AMPT-SM model, respectively. The solid and dashed bands represent the ratios at the most central (0–5%) and most peripheral (60–80%) centrality classes, respectively.

ter through various baryon-baryon, meson-baryon, and meson-meson scatterings. This leads to a corresponding rise in the observed ϕ/π ratio at intermediate p_T . The difference in ϕ/π ratios in AMPT-SM and EPOS4 might also be attributed to the influence of the Lund string fragmentation parameters on the yields of strange quarks carrying hadron-like ϕ mesons. AMPT-SM may have implemented these parameters more effectively, leading to a stronger preference for strange quark hadronization than in EPOS4 [65]. EPOS4 does not include a coalescence mechanism, and the ϕ/π ratio reflects the complex interplay between core-corona separation, hydrodynamics, collective flow, and particle production mechanisms across different p_T ranges. Ξ/π ratios also show strong centrality dependence at the intermediate p_T in all models. Similar to the Λ/π ratios, the Ξ/π ratios exhibit a pronounced peak with a maximum of around 2–3 GeV/ c in most central collisions. A slightly higher prediction of Ξ/π ratios in 0–5% central collisions in EPOS4 as compared to AMPT-SM may be due to implementing flow effects.

Figure 6 shows p_T -differential p/π and Λ/K_S^0 in the most central (0–5%) and peripheral (60–80%) O + O collisions at $\sqrt{s_{NN}} = 7$ TeV using all models. The p_T -differential p/π (the lightest baryon to the lightest meson) ratio serves as a proxy of the relative production of baryons compared to mesons. Both ratios show a strong centrality dependence at intermediate p_T . A similar peak around 2–3 GeV/ c in most central collisions is observed in p/π ratios from EPOS4 and AMPT-SM at intermediate p_T . It is also observed that the trend appears to be

a plateau at intermediate p_T for central and peripheral collisions similar to that observed in p + p, p + Pb, and Pb+Pb collisions at the LHC [8, 59–63]. Λ/K_S^0 ratios also exhibits strong centrality dependence at intermediate p_T .

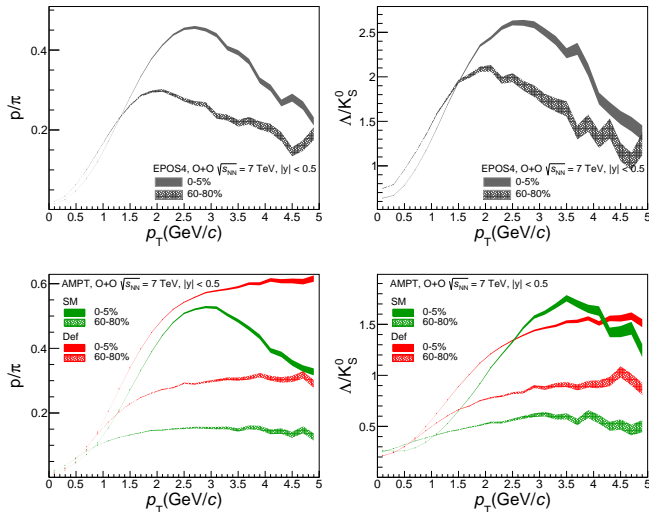


FIG. 6. (Color online) p_T -differential baryon-to-meson (p/π and Λ/K_S^0) ratios in most central (0–5%) and the most peripheral (60–80%) O + O collisions using EPOS4 (Top) and AMPT (bottom). Black color is used for EPOS4, whereas the red and green color represent AMPT-Def and the AMPT-SM model, respectively. Solid and dashed bands represent the ratios at the most central (0–5%) and most peripheral (60–80%) centrality class respectively.

The enhancement in Λ/K_S^0 in 0–5% central collisions from EPOS4 is significantly larger than that predicted by the AMPT-SM model despite having a similar distribution. This discrepancy may be attributed to the strong radial flow implemented in EPOS4, which affects baryons like Λ at higher multiplicities. In contrast, AMPT incorporates a certain degree of flow effects. This result aligns closely with the observed collision dynamics at this center-of-mass energy, indicating that the EPOS4 treatment of strangeness production mechanisms, especially for these particles, shows better consistency with the existing experimental data [37, 55].

IV. CONCLUSIONS

We present predictions of various observables for (multi)strange hadrons (K_S^0 , $\Lambda(\bar{\Lambda})$, $\Xi^-(\bar{\Xi}^+)$, ϕ , and $\Omega^-(\bar{\Omega}^+)$) in O + O collisions at $\sqrt{s_{NN}} = 7$ TeV using the recently updated hydrodynamic-based EPOS4 and two different versions the AMPT model. These models have been utilized to investigate the transverse momentum (p_T) spectra, multiplicity dependence of particle yield (dN/dy), yield ratio of various strange meson and baryon relative to pions. EPOS4 performs well in pre-

dicting the strangeness enhancement, while AMPT does not. However, none of the models quantitatively describe the strangeness enhancement. A clear final state multiplicity overlap is observed with p + p, p + Pb and Pb + Pb collisions from all the models. The p_T -differential strange hadron to pion ratios shows a clear centrality dependence. AMPT predicts strong enhancement in ϕ/π ratio as compared to EPOS4, due to the effective implementation of the Lund string fragmentation parameters leading to a stronger preference for strange quark hadronization and may effect the yield of ϕ mesons in comparison with EPOS4. The larger enhancement in Λ/K_S^0 ratio at the intermediate- p_T region from EPOS4 compared to AMPT might be attributed to the implementation of full hydrodynamic flow in EPOS4 which seems to play an important role and appears to be significantly more effective in reproducing the existing experimental data, while AMPT incorporates some flow effects. The upcoming data on O + O collisions at the LHC will be helpful in constraining and refining the model parameters.

V. ACKNOWLEDGEMENTS

Authors would like to thank W. J. Llope and S.K. Grossberndt for careful reading and discussions. S. Kaban acknowledge partial support from the Agencia Nacional de Investigación y Desarrollo de Chile (ANID), Chile, with the grants ANID PIA/APOYO AFB230003, Chile, and ANID FONDECYT regular No 1230987, Chile.

A. References

- [1] N. Cabibbo and G. Parisi, “Exponential Hadronic Spectrum and Quark Liberation”, *Phys. Lett. B* **59** (1975) 67–69.
- [2] E. V. Shuryak, “Quark-Gluon Plasma and Hadronic Production of Leptons, Photons and Psions”, *Phys. Lett. B* **78** (1978) 150.
- [3] E. Laermann and O. Philipsen, “The Status of lattice QCD at finite temperature”, *Ann. Rev. Nucl. Part. Sci.* **53** (2003) 163–198, [arXiv:hep-ph/0303042](#).
- [4] P. Romatschke and U. Romatschke, *Relativistic Fluid Dynamics In and Out of Equilibrium*. Cambridge Monographs on Mathematical Physics. Cambridge University Press, 5, 2019. [arXiv:1712.05815 \[nucl-th\]](#).
- [5] U. Heinz and R. Snellings, “Collective flow and viscosity in relativistic heavy-ion collisions”, *Ann. Rev. Nucl. Part. Sci.* **63** (2013) 123–151, [arXiv:1301.2826 \[nucl-th\]](#).
- [6] J. Rafelski and B. Muller, “Strangeness Production in the Quark - Gluon Plasma”, *Phys. Rev. Lett.* **48** (1982) 1066. [Erratum: *Phys.Rev.Lett.* 56, 2334 (1986)].
- [7] **STAR** Collaboration, J. Adam *et al.*, “Strange hadron production in Au+Au collisions at $\sqrt{s_{NN}} = 7.7, 11.5, 19.6, 27, \text{ and } 39$ GeV”, *Phys. Rev. C* **102** no. 3, (2020) 034909, [arXiv:1906.03732 \[nucl-ex\]](#).

- [8] **ALICE** Collaboration, J. Adam *et al.*, “Enhanced production of multi-strange hadrons in high-multiplicity proton-proton collisions”, *Nature Phys.* **13** (2017) 535–539, [arXiv:1606.07424 \[nucl-ex\]](#).
- [9] **CMS** Collaboration, V. Khachatryan *et al.*, “Evidence for collectivity in pp collisions at the LHC”, *Phys. Lett. B* **765** (2017) 193–220, [arXiv:1606.06198 \[nucl-ex\]](#).
- [10] **ALICE** Collaboration, S. Acharya *et al.*, “Investigations of Anisotropic Flow Using Multiparticle Azimuthal Correlations in pp, p-Pb, Xe-Xe, and Pb-Pb Collisions at the LHC”, *Phys. Rev. Lett.* **123** no. 14, (2019) 142301, [arXiv:1903.01790 \[nucl-ex\]](#).
- [11] K. Redlich and A. Tounsi, “Strangeness enhancement and energy dependence in heavy ion collisions”, *Eur. Phys. J. C* **24** (2002) 589–594, [arXiv:hep-ph/0111261](#).
- [12] V. Vovchenko, B. Dönigus, and H. Stoecker, “Canonical statistical model analysis of p-p, p-Pb, and Pb-Pb collisions at energies available at the CERN Large Hadron Collider”, *Phys. Rev. C* **100** no. 5, (2019) 054906, [arXiv:1906.03145 \[hep-ph\]](#).
- [13] **ALICE** Collaboration, S. Acharya *et al.*, “Multiplicity dependence of light-flavor hadron production in pp collisions at $\sqrt{s} = 7$ TeV”, *Phys. Rev. C* **99** no. 2, (2019) 024906, [arXiv:1807.11321 \[nucl-ex\]](#).
- [14] R. Hagedorn and K. Redlich, “Statistical Thermodynamics in Relativistic Particle and Ion Physics: Canonical or Grand Canonical?”, *Z. Phys. C* **27** (1985) 541.
- [15] C. M. Ko, V. Koch, Z.-w. Lin, K. Redlich, M. A. Stephanov, and X.-N. Wang, “Kinetic equation with exact charge conservation”, *Phys. Rev. Lett.* **86** (2001) 5438–5441, [arXiv:nucl-th/0010004](#).
- [16] S. Porteboeuf, T. Pierog, and K. Werner, “Producing hard processes regarding the complete event: The epos event generator”, 2010.
- [17] F. Becattini and J. Manninen, “Strangeness production from SPS to LHC”, *J. Phys. G* **35** (2008) 104013, [arXiv:0805.0098 \[nucl-th\]](#).
- [18] J. Aichelin and K. Werner, “Centrality Dependence of Strangeness Enhancement in Ultrarelativistic Heavy Ion Collisions: A Core-Corona Effect”, *Phys. Rev. C* **79** (2009) 064907, [arXiv:0810.4465 \[nucl-th\]](#). [Erratum: *Phys.Rev.C* 81, 029902 (2010)].
- [19] Y. Kanakubo, Y. Tachibana, and T. Hirano, “Unified description of hadron yield ratios from dynamical core-corona initialization”, *Phys. Rev. C* **101** no. 2, (2020) 024912, [arXiv:1910.10556 \[nucl-th\]](#).
- [20] Y. Kanakubo, Y. Tachibana, and T. Hirano, “Interplay between core and corona components in high-energy nuclear collisions”, *Phys. Rev. C* **105** no. 2, (2022) 024905, [arXiv:2108.07943 \[nucl-th\]](#).
- [21] T. Sjostrand, S. Mrenna, and P. Z. Skands, “A Brief Introduction to PYTHIA 8.1”, *Comput. Phys. Commun.* **178** (2008) 852–867, [arXiv:0710.3820 \[hep-ph\]](#).
- [22] C. Bierlich and J. R. Christiansen, “Effects of color reconnection on hadron flavor observables”, *Phys. Rev. D* **92** no. 9, (2015) 094010, [arXiv:1507.02091 \[hep-ph\]](#).
- [23] T. Pierog, I. Karpenko, J. M. Katzy, E. Yatsenko, and K. Werner, “EPOS LHC: Test of collective hadronization with data measured at the CERN Large Hadron Collider”, *Phys. Rev. C* **92** no. 3, (2015) 034906, [arXiv:1306.0121 \[hep-ph\]](#).
- [24] Z.-W. Lin and L. Zheng, “Further developments of a multi-phase transport model for relativistic nuclear collisions”, *Nucl. Sci. Tech.* **32** no. 10, (2021) 113, [arXiv:2110.02989 \[nucl-th\]](#).
- [25] J. Brewer, A. Mazeliauskas, and W. van der Schee, “Opportunities of OO and pO collisions at the LHC”, in *Opportunities of OO and pO collisions at the LHC*. 3, 2021. [arXiv:2103.01939 \[hep-ph\]](#).
- [26] **ALICE** Collaboration, “ALICE physics projections for a short oxygen-beam run at the LHC”, .
- [27] S. H. Lim, J. Carlson, C. Loizides, D. Lonardonì, J. E. Lynn, J. L. Nagle, J. D. Orjuela Koop, and J. Ouellette, “Exploring New Small System Geometries in Heavy Ion Collisions”, *Phys. Rev. C* **99** no. 4, (2019) 044904, [arXiv:1812.08096 \[nucl-th\]](#).
- [28] M. Rybczyński and W. Broniowski, “Glauber Monte Carlo predictions for ultrarelativistic collisions with ^{16}O ”, *Phys. Rev. C* **100** no. 6, (2019) 064912, [arXiv:1910.09489 \[hep-ph\]](#).
- [29] S. Huang, Z. Chen, J. Jia, and W. Li, “Disentangling contributions to small-system collectivity via scans of light nucleus-nucleus collisions”, *Phys. Rev. C* **101** no. 2, (2020) 021901, [arXiv:1904.10415 \[nucl-ex\]](#).
- [30] M. D. Sievert and J. Noronha-Hostler, “CERN Large Hadron Collider system size scan predictions for PbPb, XeXe, ArAr, and OO with relativistic hydrodynamics”, *Phys. Rev. C* **100** no. 2, (2019) 024904, [arXiv:1901.01319 \[nucl-th\]](#).
- [31] B. Schenke, C. Shen, and P. Tribedy, “Running the gamut of high energy nuclear collisions”, *Phys. Rev. C* **102** no. 4, (2020) 044905, [arXiv:2005.14682 \[nucl-th\]](#).
- [32] B. G. Zakharov, “Jet quenching from heavy to light ion collisions”, *JHEP* **09** (2021) 087, [arXiv:2105.09350 \[hep-ph\]](#).
- [33] A. Huss, A. Kurkela, A. Mazeliauskas, R. Paatelainen, W. van der Schee, and U. A. Wiedemann, “Predicting parton energy loss in small collision systems”, *Phys. Rev. C* **103** no. 5, (2021) 054903, [arXiv:2007.13758 \[hep-ph\]](#).
- [34] D. Behera, S. Deb, C. R. Singh, and R. Sahoo, “Characterizing nuclear modification effects in high-energy O-O collisions at energies available at the CERN Large Hadron Collider: A transport model perspective”, *Phys. Rev. C* **109** no. 1, (2024) 014902, [arXiv:2308.06078 \[hep-ph\]](#).
- [35] D. Behera, N. Mallick, S. Tripathy, S. Prasad, A. N. Mishra, and R. Sahoo, “Predictions on global properties in O+O collisions at the Large Hadron Collider using a multi-phase transport model”, *Eur. Phys. J. A* **58** no. 9, (2022) 175, [arXiv:2110.04016 \[hep-ph\]](#).
- [36] A. M. Khan, M. U. Ashraf, S. K. Malik, H. M. Alfanda, and M. U. Aslam, “Dynamics of identified particles production in oxygen-oxygen collisions at $\sqrt{(s_{NN})} = 7$ TeV using EPOS4”, [arXiv:2402.13843 \[hep-ph\]](#).
- [37] K. Werner, “Core-corona procedure and microcanonical hadronization to understand strangeness enhancement in proton-proton and heavy ion collisions in the epos4 framework”, *Physical Review C* **109** no. 1, (Jan., 2024) . <http://dx.doi.org/10.1103/PhysRevC.109.014910>.
- [38] T. Shao, J. Chen, C. M. Ko, and Z.-W. Lin, “Enhanced production of strange baryons in high-energy nuclear collisions from a multiphase transport model”, *Phys.*

- Rev. C* **102** no. 1, (2020) 014906, [arXiv:2012.10037 \[nucl-th\]](#).
- [39] Z.-W. Lin, C. M. Ko, B.-A. Li, B. Zhang, and S. Pal, “A Multi-phase transport model for relativistic heavy ion collisions”, *Phys. Rev. C* **72** (2005) 064901, [arXiv:nucl-th/0411110](#).
- [40] G.-L. Ma and Z.-W. Lin, “Predictions for $\sqrt{s_{NN}} = 5.02$ TeV Pb+Pb Collisions from a Multi-Phase Transport Model”, *Phys. Rev. C* **93** no. 5, (2016) 054911, [arXiv:1601.08160 \[nucl-th\]](#).
- [41] K. Werner and B. Guiot, “Perturbative QCD concerning light and heavy flavor in the EPOS4 framework”, *Phys. Rev. C* **108** no. 3, (2023) 034904, [arXiv:2306.02396 \[hep-ph\]](#).
- [42] K. Werner, “Revealing a deep connection between factorization and saturation: New insight into modeling high-energy proton-proton and nucleus-nucleus scattering in the EPOS4 framework”, *Phys. Rev. C* **108** no. 6, (2023) 064903, [arXiv:2301.12517 \[hep-ph\]](#).
- [43] X.-N. Wang and M. Gyulassy, “HIJING: A Monte Carlo model for multiple jet production in p p, p A and A A collisions”, *Phys. Rev. D* **44** (1991) 3501–3516.
- [44] B. Zhang, “ZPC 1.0.1: A Parton cascade for ultrarelativistic heavy ion collisions”, *Comput. Phys. Commun.* **109** (1998) 193–206, [arXiv:nucl-th/9709009](#).
- [45] B.-A. Li and C. M. Ko, “Formation of superdense hadronic matter in high-energy heavy ion collisions”, *Phys. Rev. C* **52** (1995) 2037–2063, [arXiv:nucl-th/9505016](#).
- [46] Z.-w. Lin and C. M. Ko, “Partonic effects on the elliptic flow at RHIC”, *Phys. Rev. C* **65** (2002) 034904, [arXiv:nucl-th/0108039](#).
- [47] A. Bzdak and G.-L. Ma, “Elliptic and triangular flow in p+Pb and peripheral Pb+Pb collisions from parton scatterings”, *Phys. Rev. Lett.* **113** no. 25, (2014) 252301, [arXiv:1406.2804 \[hep-ph\]](#).
- [48] G.-L. Ma and A. Bzdak, “Long-range azimuthal correlations in proton–proton and proton–nucleus collisions from the incoherent scattering of partons”, *Phys. Lett. B* **739** (2014) 209–213, [arXiv:1404.4129 \[hep-ph\]](#).
- [49] Werner, K., Guiot, B., Karpenko, Iu., Pierog, T., Sophys, G., and Stefaniak, M., “EPOS”, *EPJ Web Conf.* **208** (2019) 11005. <https://doi.org/10.1051/epjconf/201920811005>.
- [50] C. R. Allton, S. Ejiri, S. J. Hands, O. Kaczmarek, F. Karsch, E. Laermann, C. Schmidt, and L. Scorzato, “The QCD thermal phase transition in the presence of a small chemical potential”, *Phys. Rev. D* **66** (2002) 074507, [arXiv:hep-lat/0204010](#).
- [51] M. Bleicher *et al.*, “Relativistic hadron hadron collisions in the ultrarelativistic quantum molecular dynamics model”, *J. Phys. G* **25** (1999) 1859–1896, [arXiv:hep-ph/9909407](#).
- [52] S. A. Bass *et al.*, “Microscopic models for ultrarelativistic heavy ion collisions”, *Prog. Part. Nucl. Phys.* **41** (1998) 255–369, [arXiv:nucl-th/9803035](#).
- [53] H. Petersen, J. Steinheimer, G. Burau, M. Bleicher, and H. Stöcker, “A Fully Integrated Transport Approach to Heavy Ion Reactions with an Intermediate Hydrodynamic Stage”, *Phys. Rev. C* **78** (2008) 044901, [arXiv:0806.1695 \[nucl-th\]](#).
- [54] A. G. Knospe, C. Markert, K. Werner, J. Steinheimer, and M. Bleicher, “Hadronic resonance production and interaction in partonic and hadronic matter in the EPOS3 model with and without the hadronic afterburner UrQMD”, *Phys. Rev. C* **93** no. 1, (2016) 014911, [arXiv:1509.07895 \[nucl-th\]](#).
- [55] K. Werner, B. Guiot, I. Karpenko, and T. Pierog, “Analysing radial flow features in p-Pb and p-p collisions at several TeV by studying identified particle production in EPOS3”, *Phys. Rev. C* **89** no. 6, (2014) 064903, [arXiv:1312.1233 \[nucl-th\]](#).
- [56] S. Tripathy, S. K. Tiwari, M. Younus, and R. Sahoo, “Elliptic flow in Pb+Pb collisions at $\sqrt{s_{NN}} = 2.76$ TeV at the LHC using Boltzmann transport equation with non-extensive statistics”, *Eur. Phys. J. A* **54** no. 3, (2018) 38, [arXiv:1709.06354 \[hep-ph\]](#).
- [57] R. Rath, S. Tripathy, R. Sahoo, S. De, and M. Younus, “Identified particle production in Xe+Xe collisions at $\sqrt{s_{NN}} = 5.44$ TeV using a multiphase transport model”, *Phys. Rev. C* **99** no. 6, (2019) 064903, [arXiv:1812.05041 \[hep-ph\]](#).
- [58] K. Werner, “Core-corona separation in ultra-relativistic heavy ion collisions”, *Phys. Rev. Lett.* **98** (2007) 152301, [arXiv:0704.1270 \[nucl-th\]](#).
- [59] **ALICE** Collaboration, B. B. Abelev *et al.*, “Multi-strange baryon production at mid-rapidity in Pb-Pb collisions at $\sqrt{s_{NN}} = 2.76$ TeV”, *Phys. Lett. B* **728** (2014) 216–227, [arXiv:1307.5543 \[nucl-ex\]](#). [Erratum: *Phys.Lett.B* 734, 409–410 (2014)].
- [60] **ALICE** Collaboration, B. B. Abelev *et al.*, “Multiplicity Dependence of Pion, Kaon, Proton and Lambda Production in p-Pb Collisions at $\sqrt{s_{NN}} = 5.02$ TeV”, *Phys. Lett. B* **728** (2014) 25–38, [arXiv:1307.6796 \[nucl-ex\]](#).
- [61] **ALICE** Collaboration, J. Adam *et al.*, “Multi-strange baryon production in p-Pb collisions at $\sqrt{s_{NN}} = 5.02$ TeV”, *Phys. Lett. B* **758** (2016) 389–401, [arXiv:1512.07227 \[nucl-ex\]](#).
- [62] **ALICE** Collaboration, J. Adam *et al.*, “ $K^*(892)^0$ and $\phi(1020)$ meson production at high transverse momentum in pp and Pb-Pb collisions at $\sqrt{s_{NN}} = 2.76$ TeV”, *Phys. Rev. C* **95** no. 6, (2017) 064606, [arXiv:1702.00555 \[nucl-ex\]](#).
- [63] **ALICE** Collaboration, B. Abelev *et al.*, “Production of $K^*(892)^0$ and $\phi(1020)$ in pp collisions at $\sqrt{s} = 7$ TeV”, *Eur. Phys. J. C* **72** (2012) 2183, [arXiv:1208.5717 \[hep-ex\]](#).
- [64] Y. He and Z.-W. Lin, “Improved Quark Coalescence for a Multi-Phase Transport Model”, *Phys. Rev. C* **96** no. 1, (2017) 014910, [arXiv:1703.02673 \[nucl-th\]](#).
- [65] K. Tiwari and M. Nasim, “Constraining input parameters of AMPT model with ϕ meson production”, *Nucl. Phys. A* **999** (2020) 121751, [arXiv:2002.01201 \[nucl-th\]](#).